Line defects of *M*-plane GaN grown on γ-$LiAlO_2$ by plasma-assisted molecular beam epitaxy

Ikai Lo,[1,a)] Chia-Ho Hsieh,[1] Yen-Liang Chen,[1] Wen-Yuan Pang,[1] Yu-Chi Hsu,[1] Jih-Chen Chiang,[1] Ming-Chi Chou,[1] Jenn-Kai Tsai,[2] and D. M. Schaadt[3]
[1]*Department of Physics, Institute of Material Science and Engineering, Center for Nanoscience and Nanotechnology, National Sun Yat-Sen University, Kaohsiung, Taiwan 80424, Republic of China*
[2]*National Formosa University, Hu-Wei, Yun-Lin, Taiwan 63208, Republic of China*
[3]*Institut für Angewandte Physik/Center for Functional Nanostructures, Universität Karlsruhe, 76131 Karlsruhe, Germany*

(Received 9 March 2008; accepted 19 April 2008; published online 19 May 2008)

The edge and threading dislocations of *M*-plane GaN epilayers grown on γ-$LiAlO_2$ have been studied by high-resolution transmission electron microscope. We found that edge dislocations were grown in $[1\bar{1}00]$ direction while threading dislocations were generated along $\boldsymbol{a}_1$ or $-\boldsymbol{a}_2$ axes. We also observed a single stacking fault in the *M*-plane GaN epilayer. © *2008 American Institute of Physics*. [DOI: 10.1063/1.2924288]

GaN has attracted much attention in the current decade due to its potential application to blue light optoelectronic devices and high-performance electronic devices.[1–4] When GaN epilayer is grown on a sapphire (0001), a high density of threading dislocations can be induced in the *c*-plane GaN epilayer along [0001] direction.[5,6] Nakamura *et al.* showed that the GaN-based light-emitting device was insensitive to the threading dislocation,[7] however, other studies indicated that the extended line defects did affect the optical[8–10] or electrical[11–15] performance of two-dimensional (2D) electron gas. In addition, Hino *et al.* showed that screw and mixed dislocations, were acting as nonradiative centers but edge dislocations were optically inactive.[16] On the contrary, Cherns *et al.* showed that both edge and screw dislocations acted as nonradiative centers in *c*-plane GaN/InGaN quantum wells.[17] The optical properties of line defects are still inconclusive for the *c*-plane GaN epilayer grown on sapphire. Moreover, a strong electrostatic field is induced at the heterointerface of AlGaN/GaN as grown on sapphire, due to the spontaneous and piezoelectric polarizations along the polar *c* axis.[18] The strong electrostatic field tilts the band structure of AlGaN/GaN quantum well, resulting in a quench of photoluminescence (PL). In order to avoid the internal electrostatic field, Waltereit *et al.* demonstrated that AlGaN/GaN grown along the $[1\bar{1}00]$ direction on a γ-$LiAlO_2$ substrate significantly enhanced luminous quantum efficiency.[19] The tetragonal γ-$LiAlO_2$ (LAO) offers a nearly lattice-matched substrate to grow *M*-plane GaN $(1\bar{1}00)$ on a rectangular anionic basal plane in which $a_{LAO} \cong b_{LAO} \cong c_{GaN}$ and $c_{LAO} \cong 2a_{GaN}$, Fig. 1(a). The heterointerface of *M*-plane AlGaN/GaN is nonpolar, and hence the internal electrostatic field due to piezoelectric polarization is eliminated along the growth direction. The absence of piezoelectric field provides a flatband quantum well structure to enhance the luminous quantum efficiency for optoelectronic devices.[20–22] Therefore, in *M*-plane GaN, the detailed information of dislocation is necessary for the understanding of its role in optical and electronic properties.

Three GaN samples were grown on high-quality γ-$LiAlO_2(100)$ substrate by plasma-assisted molecular beam epitaxy (MBE). The MBE system was used to grow GaN nanorods on Si(111) substrate,[23] GaN films on sapphire,[24] and nanopillars on γ-$LiAlO_2$.[25] The growth of GaN epilayer was performed with a standard effusion cell for Ga evaporation and an rf-plasma cell for N_2-plasma source. In this study, we grew GaN epilayers on γ-$LiAlO_2$ substrate in the absence of a low-temperature GaN buffer layer. A 2 in. $LiAlO_2$ wafer was cut into four quarters for substrate preparation. The $LiAlO_2$ substrate, mounted on a rotating sample holder, was exposed to N_2-plasma 10 min for nitridation at 500 °C. After nitridation, GaN epilayers were grown at 600 °C for 4 h with different N/Ga flux ratios (as measured by beam equivalent pressure): N/Ga=19.7 for sample A, N/Ga=30.0 for sample B, and N/Ga=38.2 for sample C. The epitaxial surface was developed with nucleation, aggregation, and coalescence to form a striplike terrace along the lateral orientation $[11\bar{2}0]_{GaN} \| [001]_{LAO}$. From our previous study, we showed that the low ratio of N/Ga flux is favorable for 2D-like *M*-plane growth, while the high ratio leads to easier growth of three-dimensional (3D)-like *c*-plane nanopillars.[25] When the nucleation of rectangular basal plane (*M*-plane) predominated that of hexagonal basal plane

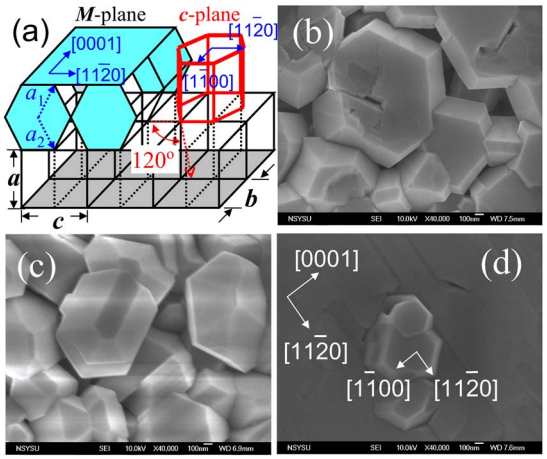

FIG. 1. (Color online) (a) Schematic diagram for two-orientation GaN (*M*-plane and *c*-plane) grown on γ-$LiAlO_2$ substrate. The SEM images of the morphology at side areas of (b) sample A, (c) sample B, and (d) sample C, respectively. The scale bar of the SEM images is 100 nm.

a)Electronic mail: ikailo@mail.phys.nsysu.edu.tw.

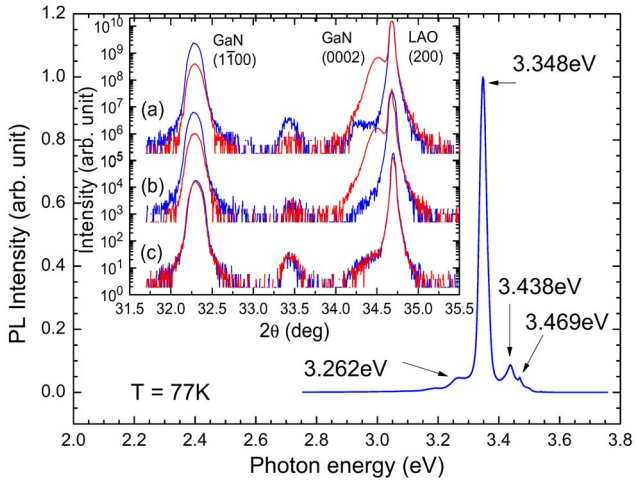

FIG. 2. (Color online) PL spectrum of sample A measured at 77 K. In the inset, XRD patterns for central (blue) and side (red) areas of samples (a) A, (b) B, and (c) C, respectively.

(*c*-plane), the growth of *M*-plane surface became favorable, resulting in striplike terraces of *M*-plane GaN. The growth of *M*-plane surface along the lateral [11$\bar{2}$0] direction failed to coalesce with a *c*-plane hexagonal nanocrystal, yielding a 120° angle between them. Since the growth rate in the *z* direction for striplike *M*-plane GaN is different from that for compact hexagonal *c*-plane GaN, two-orientation GaN growth (2D *M*-plane and 3D *c*-plane) is then constructed. The schematic diagram is shown in Fig. 1(a). When we grew the GaN epilayers, the *M*-plane 2D terraces were constructed at the central area of the samples, while 3D *c*-plane nanocrystals survived mostly at the side area. Scanning electron microscope (SEM) images of the side areas of samples A, B, and C are shown in Figs. 1(b)–1(d), respectively. The axis orientations of *M*-plane and *c*-plane GaN in sample C are plotted on Fig. 1(d), which are consistent with the configuration in Fig. 1(a) and reconfirm the two-orientation GaN growth.[25] To check the crystal structure we performed x-ray diffraction (XRD) measurement focused on both central and side areas of these samples. The XRD results were shown in the inset of Fig. 2. The peaks at 2θ=34.68° and 32.29° for both central and side areas are corresponding to the diffraction of $LiAlO_2$ (200) and *M*-plane GaN (1$\bar{1}$00), respectively. However, the peak of 2θ=34.51°, due to the diffraction of *c*-plane GaN (0002), is clearly observed at the side areas of samples A and B but less in sample C. It is noted that a peak at 2θ=33.42°, induced by AlN (1$\bar{1}$00) diffraction, was slightly visible in the XRD patterns for samples A and C, in which the aluminum atoms probably came from the substrate.

Dislocation is a line defect extended to the crystal to relieve the strain induced by lattice mismatch. It can be characterized by a Burgers vector ($\boldsymbol{b}$) and a dislocation line ($\boldsymbol{l}$). Based on the angle between Burgers vector and dislocation line, the line defects can be categorized into three types: edge, screw, and mixed dislocations.[26] The Burgers vector is perpendicular to the line of edge dislocation ($\boldsymbol{b} \perp \boldsymbol{l}_{\text{edge}}$) but parallel to that of screw dislocation ($\boldsymbol{b} \| \boldsymbol{l}_{\text{screw}}$). In the general case, the dislocation shows a mixed character of both edge and screw types to form a kind of threading dislocation. High-resolution TEM (HRTEM) and selected area electron diffraction (SAD) measurements were used to analyze the atomic structures of the extended line defects. A specimen for TEM measurement was cut by focused ion beam from the central area of sample A with a cleavage plane of GaN(0001)$\|$$LiAlO_2$(010), in which a *c*-plane GaN nanocrystal was embedded between two *M*-plane GaN terraces. A cross-sectional TEM image is shown in Fig. 3(a). The SAD patterns taken along the direction of $[0001]_{\text{GaN}} \| [010]_{\text{LAO}}$ at the points located at DP01—DP04 are shown in Figs. 3(b)–3(e). The SAD pattern taken at point DP01 indicates the diffraction spots of *c*-plane GaN along the [1$\bar{1}$00] direction, Fig. 3(b). The SAD pattern taken at point DP02 shows the diffraction spots of *M*-plane GaN along [0001] direction, Fig. 3(c). The SAD patterns taken at points DP01 and DP02 are supported by the morphology in SEM images. In Fig. 3(d), the SAD pattern at point DP03 indicates the diffraction spots of GaN(0001)$\|$$LiAlO_2$(010), and reconfirms the heterointerface to be GaN(1$\bar{1}$00)$\|$$LiAlO_2$(100), as illustrated in Fig. 1(a). The SAD pattern taken at point DP04 represents the diffraction of γ-$LiAlO_2$ substrate along the [010] direction with different intensity of spots, Fig. 3(e). Many line defects are clearly visible in the cross-sectional TEM image. These dislocation lines can be classified to (i) the lines parallel to the direction [1$\bar{1}$00] denoted as $\boldsymbol{l}_{\text{(i)}}$, or (ii) those lines along with the prismatic axes $\boldsymbol{a}_1$ or $-\boldsymbol{a}_2$, denoted as $\boldsymbol{l}_{\text{(ii)}}$. Because the edge dislocation line is perpendicular to Burgers vector, the dislocation lines $\boldsymbol{l}_{\text{(i)}}$ are related to the edge dislocations of $\boldsymbol{l}_{\text{edge}} \| [1\bar{1}00]$ with the Burgers vector $\boldsymbol{b}=\frac{1}{3}[11\bar{2}0]$, where ($\boldsymbol{b} \perp \boldsymbol{l}_{\text{edge}}$) is shown in Fig. 3(a). The dislocation lines $\boldsymbol{l}_{\text{(ii)}}$ have the mixed characters of edge and screw types to form the threading dislocations along axes $\boldsymbol{a}_1$ or $-\boldsymbol{a}_2$. Unlike *c*-plane GaN, in which threading dislocations are vertically

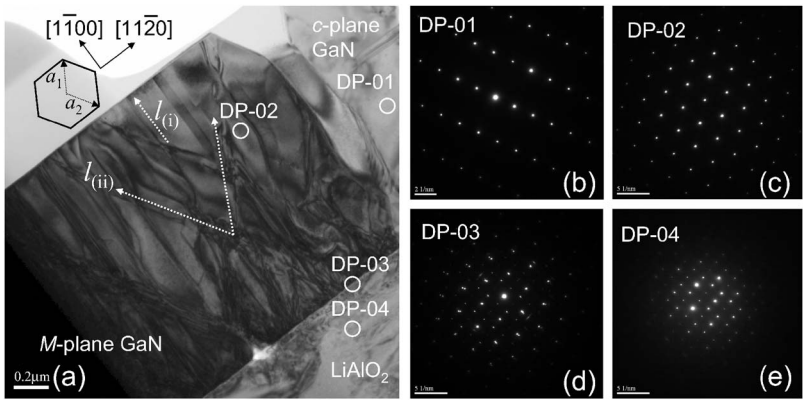

FIG. 3. (a) Cross-sectional TEM image taken along $[0001]_{\text{GaN}} \| [010]_{\text{LAO}}$ at the central area of sample A. (b) The rectangular SAD pattern taken at point DP01 indicates. (c) The prismatic SAD pattern taken at point DP02. (d) The combination of square and prismatic meshes with different intensity of SAD spots taken at point DP03. (e) The square mesh with different intensity of SAD spots taken at point DP04. The scale bar is 2 (1/nm) for (b) and 5 (1/nm) for (c–e).

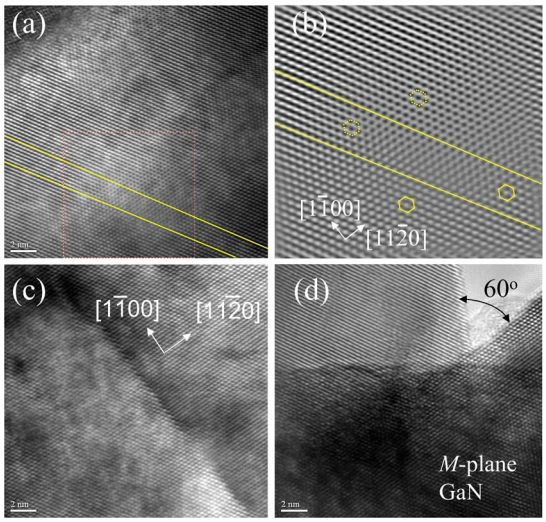

FIG. 4. (Color online) (a) TEM image of a single stacking fault taken along the [0001] direction on *M*-plane GaN. (b) IFFT pattern from the red block in (a). (c) TEM image of an edge dislocation in *M*-plane GaN. (d) TEM image of coalescence occurring at the adjacent surface of *M*-plane GaN.

grown along the [0001] direction, the threading dislocations in *M*-plane GaN are generated along with the axes of $\boldsymbol{a}_1$ or $-\boldsymbol{a}_2$ leaving a 60° V-shape of lines in the TEM image.

To investigate the atomic microstructure of the line defects, we focused the electron beam on the top region of *M*-plane GaN terrace in Fig. 3(a) for HRTEM measurement. The results of cross-sectional HRTEM images were shown in Figs. 4(a) and 4(c). A single stacking fault was detected between the lines in Fig. 4(a). The extra line was justified by the inversed fast Fourier transform (IFFT) from the TEM image. Figure 4(b) shows the IFFT pattern of the red block in Fig. 4(a). In the IFFT pattern, it is shown that five lattice lines turned into six lattice lines after the stacking fault. We found that the separation between the two lattice lines at the left side is greater than that at the right side. We believe that the epitaxial strain was relaxed after the generation of stacking fault. The stacking fault associated with screw and edge dislocations to form threading dislocation lines. The atomic microstructure of an edge dislocation line is shown in Fig. 4(c), where the dislocation line ($\boldsymbol{l}_{\text{edge}} \| [1\bar{1}00]$) and Burgers vector ($\boldsymbol{b} \| [11\bar{2}0]$) are shown as well. In addition to the line defects, we also examined the microstructure of grain boundary of *M*-plane GaN and the result is shown in Fig. 4(d). It is found that the prismatic planar defects with stacking faults were formed at the boundary of *M*-plane GaN. The prismatic planar defect originated from misfit dislocations as well as stacking faults are not responsible for strain relief.[27] In addition, we also observed a clear atomic microstructure of coalescence at the adjacent surfaces of *M*-plane GaN. The coalescence occurred after the prismatic planar defects and created a 60° angle between the surfaces. To evaluate the optical properties of the defects, we performed PL measurement at 77 K on sample A, and the results were shown in Fig. 2. The intensity of the major peak at 3.348 eV was strongly reduced when the temperature increased and was attributed to donor-to-acceptor pair transition.[28] The second peak at 3.438 eV was related to the emission from neutral donor-bound exciton (D^0X). The other peaks (3.262 and 3.469 eV) probably originated from the emissions of excitons bound to the structural defects as proposed by Calleja *et al.*[29] The PL spectrum reveals a variety of the defect levels in the sample, which is consistent with the results of the microstructure observed by TEM.

The authors thank M. H. Gau, Y. I. Chang, and M. W. Sham for their assistance. The project was supported by National Science Council of Taiwan. The authors are grateful to W. C. Mitchel and M. Mah for their help and AFOSR/AOARD, USAF, for financial support.

[1] S. Nakamura, M. Senoh, N. Iwasa, S.-I. Nagahama, T. Yamada, T. Matsushita, Y. Sugimto, and H. Kiyoku, Appl. Phys. Lett. **70**, 1417 (1997).
[2] C. Rivera, P. Misra, J. L. Pau, E. Munoz, O. Brandt, H. T. Grahn, and K. H. Ploog, Appl. Phys. Lett. **88**, 213507 (2006).
[3] I. Lo, W. T. Wang, M. H. Gao, J. K. Tsai, S. F. Tsay, and J.-C. Chiang, Appl. Phys. Lett. **88**, 082108 (2006).
[4] I. Lo, M. H. Gau, J. K. Tsai, Y. L. Chen, Z. J. Chang, W. T. Wang, J. C. Chiang, T. Aggerstam, and S. Lourdudoss, Phys. Rev. B **75**, 245307 (2007).
[5] S. D. Lester, F. A. Ponce, M. G. Crawford, and D. A. Steigerwald, Appl. Phys. Lett. **66**, 1249 (1995).
[6] W. Qian, M. Skowronski, M. Degraef, K. Doverspike, L. B. Rowland, and D. K. Gaskill, Appl. Phys. Lett. **66**, 1252 (1995).
[7] S. Nakamura, T. Mukai, and M. Senoh, Appl. Phys. Lett. **64**, 1687 (1994).
[8] F. A. Ponce, D. P. Bour, W. Gotz, and P. J. Wright, Appl. Phys. Lett. **68**, 57 (1996).
[9] S. J. Rosner, E. C. Carr, M. L. Ludowise, G. Girolami, and H. I. Erikson, Appl. Phys. Lett. **70**, 420 (1997).
[10] J. Y. Shi, L. P. Yu, Y. Z. Wang, G. Y. Zhang, and H. Zhang, Appl. Phys. Lett. **80**, 2293 (2002).
[11] I. Lo, K. Y. Hsieh, S. L. Hwang, L. W. Tu, W. C. Mitchel, and A. W. Saxler, Appl. Phys. Lett. **74**, 2167 (1999).
[12] P. J. Hansen, Y. E. Strausser, A. N. Erickson, E. J. Tarsa, P. Kozodoy, E. G. Brazel, J. P. Ibbetson, and U. Mishra, Appl. Phys. Lett. **72**, 2247 (1998).
[13] P. Kozodoy, J. P. Ibbetson, H. Marchand, P. T. Fini, S. Keller, J. S. Speck, S. P. Enbaars, and U. K. Mishra, Appl. Phys. Lett. **73**, 975 (1998).
[14] I. Lo, J. K. Tsai, W. J. Yao, P. C. Ho, L. W. Tu, T. C. Chang, S. Elhamri, W. C. Mitchel, K. Y. Hsieh, J. H. Huang, H. L. Huang, and W. C. Tsai, Phys. Rev. B **65**, 161306 (2002).
[15] I. Lo, J. K. Tsai, M. H. Gau, Y. L. Chen, Z. J. Chang, W. T. Wang, J. C. Chiang, K. R. Wang, C.-N. Chen, T. Aggerstam, and S. Loudordoss, Phys. Rev. B **74**, 245325 (2006).
[16] T. Hino, S. Tomiya, T. Miyajima, K. Yanashima, S. Hashimoyo, and M. Ikeda, Appl. Phys. Lett. **76**, 3421 (2000).
[17] D. Cherns, S. J. Henley, and F. A. Ponce, Appl. Phys. Lett. **78**, 2691 (2001).
[18] J. A. Garrido, J. L. Sanchez-Rojas, A. Jimenez, E. Munoz, F. Omnes, and P. Gibart, Appl. Phys. Lett. **75**, 2407 (1999).
[19] P. Waltereit, O. Brandt, A. Trampert, H. T. Grahn, J. Menniger, M. Ramsteiner, M. Reiche, and K. H. Ploog, Nature (London) **406**, 865 (2000).
[20] C. Rivera, J. L. Pau, E. Munoz, P. Misra, O. Brandt, H. T. Grahn, and K. H. Ploog, Appl. Phys. Lett. **88**, 213507 (2006).
[21] P. Misra, Y. J. Sun, O. Brandt, and H. T. Grahn, Appl. Phys. Lett. **83**, 4327 (2003).
[22] C. N. Chen, S. H. Chang, M. L. Hung, J.-C. Chiang, I. Lo, W. T. Wang, M. H. Gau, H. F. Kao, and M. E. Lee, J. Appl. Phys. **101**, 043104 (2007).
[23] L. W. Tu, C. L. Hsiao, T. W. Chi, I. Lo, and K. Y. Hsieh, Appl. Phys. Lett. **82**, 1601 (2003).
[24] J. K. Tsai, I. Lo, K.-L. Chuang, L. W. Tu, J. H. Huang, C. H. Hsieh, and K.-Y. Hsieh, J. Appl. Phys. **95**, 460 (2004).
[25] C. H. Hsieh, I. Lo, M. H. Gau, Y. L. Chen, M. C. Chou, W. Y. Pang, Y. I. Chang, Y. C. Hsu, M. W. Sham, J.-C. Chiang, and J.-K. Tsai, Jpn. J. Appl. Phys. **47**, 891 (2008).
[26] D. Hull and D. J. Bacon, *Introduction to Dislocations* (Maxwell, Liverpool, UK, 1984).
[27] J. E. Northrup, Appl. Phys. Lett. **72**, 2316 (1998).
[28] J. W. Gerlach, A. Hofmann, T. Höche, F. Frost, and B. Rauschenbach, Appl. Phys. Lett. **88**, 011902 (2006).
[29] E. Calleja, M. A. Sanchez-Carcia, F. J. Sanchez, F. Calle, F. B. Naranjo, E. Munoz, U. Jahn, and K. H. Ploog, Phys. Rev. B **62**, 16826 (2000).